Chinese Chemical Letters 37 (2026) 111375

Contents lists available at ScienceDirect

Chinese Chemical Letters

journal homepage: www.elsevier.com/locate/cclet

Unusual dynamic stimuli-responsive metallamacrocyclic configurational switches

Yaqiong Kong[a,d,1], Yan Su[a,1], Yong Qian[a], Robert J. Deeth[b], Isolda Romero-Canelón[c], Zhi Su[a,*], Hong-Ke Liu[a,*], Peter J. Sadler[b,*]

[a] College of Chemistry and Materials Science, Nanjing Normal University, Nanjing 210023, China
[b] Department of Chemistry, University of Warwick, Coventry CV4 7AL, United Kingdom
[c] School of Pharmacy, Institute of Clinical Sciences, University of Birmingham, Birmingham B15 2TT, United Kingdom
[d] College of Chemistry and Materials Engineering, Chaohu University, Chaohu 238024, China

ARTICLE INFO

Article history:
Received 7 January 2025
Revised 12 May 2025
Accepted 26 May 2025
Available online 27 May 2025

Keywords:
Metallacycles
Coordination mode
Ruthenium isomer
Structure elucidation
Configuration

ABSTRACT

Specific interactions between the macrocycle backbone, solvent and counter anions control configurational interconversions of novel organoruthenium(II) metallamacrocycles [Ru(η^6-*p*-cymene)(μ_2-*m*-bitmb)Cl]$_2$·2X, *m*-bitmb = 1,3,5-trimethyl-2,4-di(imidazole-1-ylmethyl)benzene, X = Cl^- (**1·2Cl**), NO_3^- (**1·2NO$_3$**), $CF_3SO_3^-$ (**1·2CF$_3$SO$_3$**), PF_6^- (**1·2PF$_6$**), or BF_4^- (**1·2BF$_4$**). X-ray crystal structures reveal **1·2Cl** in *boat* and *chair* conformations, **1·2NO$_3$** in *twist-boat* and *chair* conformations, and **1·2CF$_3$SO$_3$** in a *chair* conformation. *Chair/boat* isomers of mono- and bis-DMSO adducts from **1·2Cl, 1·2CF$_3$SO$_3$** or **1·2NO$_3$** in DMSO/H_2O were separated and characterized. Slow anion-dependent interconversion of configurational isomers was observed in solution. Ligand field molecular mechanics and density functional theory calculations suggest an unusual macrochelate ring-opening isomerization mechanism. Such dynamic stimuli-responsive configurational changes offer scope for design of metallocycles for induced-fit recognition of biological targets.

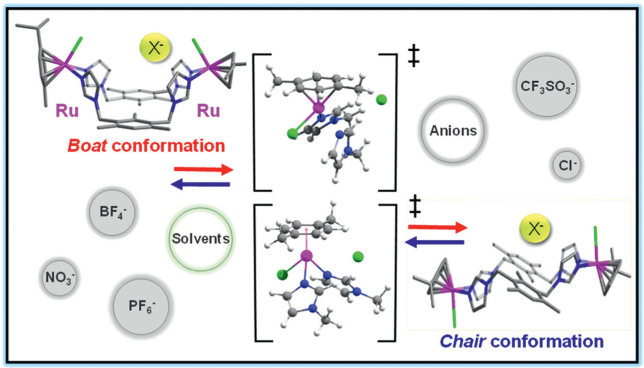
© 2025 Published by Elsevier B.V. on behalf of Chinese Chemical Society and Institute of Materia Medica, Chinese Academy of Medical Sciences.

There is much interest in the design of Ru(II) arene complexes as catalysts and anticancer complexes [1–7]. The recognition of substrates and target sites can be tailored by appropriate choice of the ligands. In complexes of the type [(η^6-arene)Ru(N,N)X], the presence of a labile ligand X, *e.g.*, Cl, allows monofunctional targeting of G bases on DNA [8,9]. With a sulfonyl group on a chelated N, the 6th coordination site becomes even more labile and a hydride acceptor/donor site in transfer hydrogenation catalysis [10,11]. In both applications, outer-sphere interactions play important roles in recognition. The NH protons on the chelated diamine H-bond with C6O of G [12–14], and bulky *N*-phenyl rings control asymmetric hydride transfer to substrates along with interactions with the arene ring [15,16]. In DNA recognition, extended arenes (*e.g.* biphenyl) can intercalate and stack with DNA bases [17,18]. Extension to di-Ru(II) complexes bridged by a flexible linker gives rise to site-specific induced-fit recognition of DNA, cross-linking between distant DNA bases, and potential protein targets [3,19,20].

Bridged multinuclear complexes offer the design of 3D architectures such as rectangles, prisms and cubes, with cavities, a variety of accessible configurations and more sophisticated recognition sites, especially involving the bridging ligands [21–23]. Stang *et al.*, for example, have reported that tetranuclear rectangular and hexanuclear trigonal prismatic metallacycles and cages containing dioxido-naphthoquinonato spacers and bis-imidazole bridging ligands self-assemble into single symmetrical and stable metallacycles and cages despite the possibility of forming isomeric conformers [24–26]. Here we use two flexible 1,3,5-trimethyl-2,4-di(imidazole-1-ylmethyl)benzene (*m*-bitmb) ligands [27], containing *N*-methylene imidazole ligands in the 2,6-positions of a central 1,3,5-trimethylbenzene unit to bridge terminal *p*-cymene (*p*-cym) Ru(II) chloride fragments (Scheme 1). We have explored the configurational space available to the 24-membered macrocyclic ring by a combination of X-ray crystallography, NMR spectroscopy, HPLC, mass spectrometry, ligand field molecular mechanics (LFMM) and density functional theory (DFT) calculations which elucidated the mechanism of configurational interconversion. We show that both counter anions and solvents play crucial roles in controlling the configuration of the macrocyclic ring. These studies of the configurational dynamics of organo-ruthenium macrocycles add a new dimension to their design features.

* Corresponding authors.
E-mail addresses: zhisu@njnu.edu.cn (Z. Su), liuhongke@njnu.edu.cn (H.-K. Liu), P.J.Sadler@warwick.ac.uk (P.J. Sadler).
[1] These authors contributed equally to this work.

https://doi.org/10.1016/j.cclet.2025.111375
1001-8417/© 2025 Published by Elsevier B.V. on behalf of Chinese Chemical Society and Institute of Materia Medica, Chinese Academy of Medical Sciences.



Scheme 1. Macrocyclic switches: A 24-membered Ru_2 metallamacrocycle with *chair*, *boat*, and *twist-boat* configurational isomers has been crystallized; its dynamic interconversion in solution is controlled by interactions between counter anions, solvent and the macrocycle backbone, with a mechanism involving Ru-ligand bond cleavage and reformation as suggested by ligand field molecular mechanics and density functional theory calculations.

Metallamacrocyclic complexes [Ru(η^6-*p*-cymene)(μ_2-*m*-bitmb)Cl]$_2$·2X, *m*-bitmb = 1,3,5-trimethyl-2,4-di(imidazole-1-ylmethyl)benzene, containing 5 different counter anions X = Cl^- (**1·2Cl**), NO_3^- (**1·2NO$_3$**), $CF_3SO_3^-$ (**1·2CF$_3$SO$_3$**), PF_6^- (**1·2PF$_6$**), or BF_4^- (**1·2BF$_4$**) were synthesized. Complex **1·2Cl** was obtained by reaction of *m*-bitmb directly with [$RuCl_2(\eta^6$-*p*-cym)]$_2$ in CH_2Cl_2/ethyl acetate, while complex **1·2CF$_3$SO$_3$** was formed by a two-step reaction. [$RuCl(\eta^6$-*p*-cym)]$_2^{2+}$, obtained from [$RuCl_2(\eta^6$-*p*-cymene)]$_2$ by adding $AgCF_3SO_3$, was reacted with the *m*-bitmb ligand. Complexes **1·2PF$_6$**, **1·2NO$_3$** and **1·2BF$_4$** were synthesized by counter-anion exchange from **1·2Cl** using the corresponding silver salts ($AgPF_6$, $AgNO_3$, $AgBF_4$, Scheme 2a).

Single crystals suitable for X-ray diffraction were obtained for **1·2Cl** from CH_2Cl_2/benzene and for **1·2NO$_3$** and **1·2CF$_3$SO$_3$** from CH_2Cl_2/toluene at ambient temperature. Yellow-block and rod-like crystals of **1·2Cl** and **1·2NO$_3$** were each hand-separated from their mother liquids. The block crystals of **1·2Cl**·0.5($CH_3COOCH_2CH_3$)·7(H_2O), and **1·2NO$_3$**·0.5(C_7H_8) have *boat* and *twist-boat* configurations, respectively (Figs. 1 and 2a). The rod-like crystals of **1·2Cl**·3(C_6H_6)·2(H_2O), **1·2NO$_3$**·(CH_2Cl_2)·H_2O·(C_7H_8), and **1·2CF$_3$SO$_3$**·2(CH_2Cl_2) have *chair* configurations for the macrocycle (Figs. 1 and 2b–d). Crystallographic data, selected bond lengths and angles are in Tables S1–S4 (Supporting information).

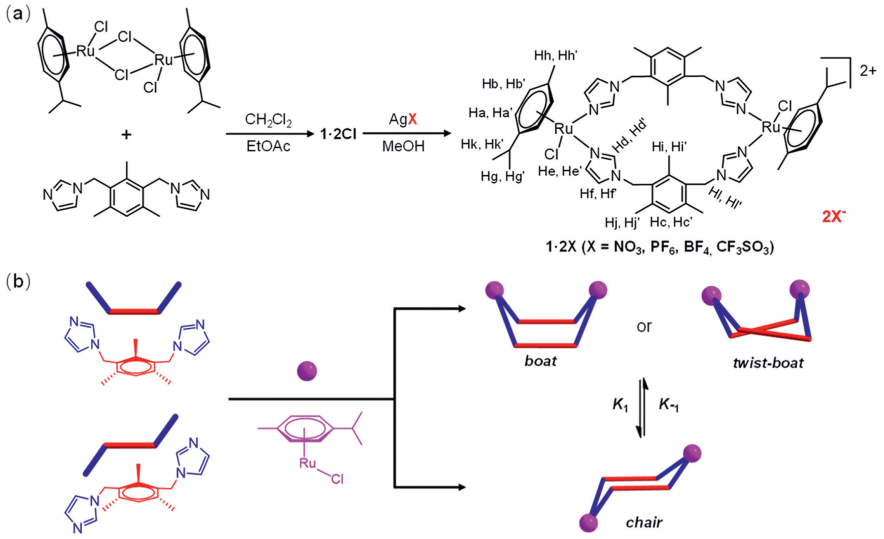
In ***chair*-1·2Cl**, the two pairs of imidazole rings of the *m*-bitmb ligands and Ru-Cl bonds face away from each other, all in *trans* arrangements (Fig. 1c). The chair structures of **1·2Cl**, **1·2NO$_3$** and **1·2CF$_3$SO$_3$** are very similar (Figs. 2b–d), with similar Ru1-Ru2 distances (12.78 Å, 12.62 Å, and 12.88 Å, respectively). The macrocyclic structure is further linked through the H-bonds between the counter anions (Cl^-) and backbone, together with solvent water molecules (Table S5 in Supporting information) involving particularly H-2′ protons of the imidazole rings (Fig. 2c).

In ***boat*-1·2Cl**, the two pairs of imidazole rings and Ru-Cl bonds face each other in a *cis* arrangement (Fig. 1b), and the Ru1-Ru2 distance shortens to 10.8 Å. The two *p*-cymene ligands are twisted from co-planarity by only 4.9°, and in both fragments, the dihedral angles between the imidazole and arene ring are 84.9°. Intermolecular π-π stacking interactions between the two Ru_2L_2 backbones induce formation of a "bottom-to-bottom" dimer, which is further connected by two Cl^- anions *via* C–H···Cl H-bonds, again involving imidazole H-2 (2.64–2.81 Å; Fig. S1 and Table S5 in Supporting information).

***Twist-boat*-1·2NO$_3$** (block crystals) has a distinct configuration (Fig. 2a). The *m*-bitmb ligands and Ru-Cl bonds still have a *cis* arrangement, but the central phenyl rings are no longer parallel, with dihedral angles between phenyl rings and imidazole rings of 64.6° and 84.9°, respectively. The Ru1-Ru2 distance shortens to 8.9 Å (c.f. 10.8 Å in ***boat*-1·2Cl**). H-bonds are also observed between NO_3^- counter anions, and backbone imidazole rings with distances of 2.47–2.55 Å (Fig. 2a and Table S5).

Thus as illustrated in Fig. 2 and Fig. S1, the non-covalent electrostatic, van de Waals, and H-bonding interactions between the cationic complexes themselves and with the counter anions and solvent of crystallization, as well as the face-to-face π-π interactions between the two *boat* form Ru_2L_2 metallamacrocycle, can play important roles in the stalilization of these conformers in the solid, crystalline state.

Next we studied the behaviour of these complexes in solution. We dissolved **1·2Cl**, **1·2NO$_3$** and **1·2CF$_3$SO$_3$** in 95 % H_2O/5 % DMSO solutions and after 24 h separated six species by reverse-phase C8 HPLC with CH_3CN/0.1 % TFA gradient elution. Remarkably three pairs of peaks were identified by ESI-HRMS (Fig. S2



Scheme 2. (a) Synthetic routes for the macrocycles, structures, and ^{1}H numbering in NMR assignments, Ha, Hb, *etc.* refer to the *boat* conformation, Ha', Hb', *etc.* refer to the *chair* conformation. (b) Diagrammatical representation of the formation of Ru_2L_2 metallomacrocycles, and configurational equilibrium for interconversion between *boat*-/*twist-boat* and *chair* isomers.

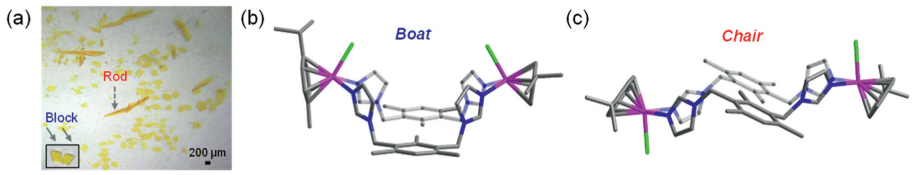


Fig. 1. (a) Mixture of block and rod-like yellow crystals from **1·2Cl** in CH_2Cl_2/benzene. (b) *Boat* structure of the metallomacrocycle in the block crystals with *cis*-oriented Ru-Cl bonds. (c) *Chair* structure of the metallomacrocycle in the rod-like crystals with *trans*-oriented Ru-Cl bonds.

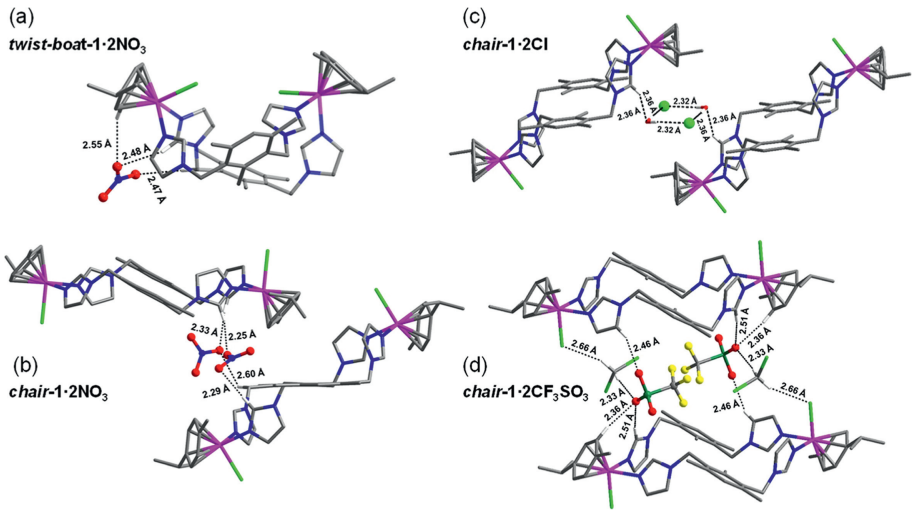


Fig. 2. Interactions between the cationic metallamacrocycle, counter anions and solvent of crystallization in (a) **1·2NO$_3$**·0.5(C_7H_8), (b) **1·2Cl**·3(C_6H_6)·2(H_2O), (c) **1·2NO$_3$**·(CH_2Cl_2)·H_2O·(C_7H_8), and (d) **1·2CF$_3$SO$_3$**·2(CH_2Cl_2). The prominent role of H-bonding is evident, between (a) NO_3^- and backbone (2.47 Å - 2.55 Å), (b) Cl^-, H_2O and backbone (2.32–2.36 Å), (c) NO_3^- and backbone (2.25–2.60 Å), and (d) $CF_3SO_3^-$, CH_2Cl_2 and backbone of *chair*-**1·2CF$_3$SO$_3$** (2.33–2.66 Å).

and Table S6 in Supporting information), assignable as isomers of [Ru(*p*-cym)(*m*-bitmb)Cl]$_2^{2+}$ (peaks 4, 5), [Ru(*p*-cym)(*m*-bitmb)Cl]$_2^{2+}$ DMSO (peaks 2, 6), and [Ru(*p*-cym)(*m*-bitmb)Cl]$_2^{2+}$ 2DMSO (peaks 1, 3), with the help of a combinatorial approach integrating NMR, single-crystal structural analysis and high-performance liquid chromatography (HPLC) methods. These DMSO molecules appear to be bound non-covalently and not direcly coordinated to Ru since MS peaks assignable to Ru-DMSO fragments could be identified and no NMR evidence for direct binding could be obtained. As shown in Fig. S3 (Supporting information), a NMR titration of **1·2Cl** with DMSO in DMF-d_7 revealed no new ^{1}H NMR signals, even after addition of 20 equiv. DMSO, only small upfield shifts of Hd/Hd' protons, suggesting weak non-coordinative interaction, confirming solvation rather than coordination.

The NMR spectra of these **1·2X** complexes showed a dependence on solvent, counter anion, and time, Fig. 3 and Figs. S4–S22 (Supporting information). Peaks were assigned by a combination of the correlation between peaks for freshly-dissolved crystals of known configuration, their behavior over time, comparison with spectra of the as-synthesized complexes, and 2D NOESY studies (Fig. 3, Figs. S4 and S15, Tables S7–S11 in Supporting information). For example, the initial single set of peaks for crystals of ***chair*-1·2NO$_3$** gave rise to a second set over the course of a few hours assignable to the *boat* configuration (Fig. 3c). Sensitivity to solvent (DMF-d_7, and CD_3CN) of the shifts of the imidazolium (Hd, He and Hf) and central phenyl (Hc) ^{1}H resonances at low field, is evident, Figs. 3a and b, and S4, Tables S7 and S8 (Supporting information).

Similarly we recorded ^{1}H NMR spectra of fresh solutions of the other complexes. The initial *boat*:*chair* ratios differed from 3:1 for as-synthesized **1·2NO$_3$**, **1·2PF$_6$** and **1·2BF$_4$**, 2:1 for **1·2Cl**, and 1:1 for **1·2CF$_3$SO$_3$** (Figs. S5–S8). As can be seen in Fig. S9, over a period of about 120 h, all complexes reached an equilibrium ratio of *ca.* 1:1, as determined by integration of Hd(*boat*)/Hd'(*chair*) peaks, the same as for **1·2CF$_3$SO$_3$** which did not change. Treatment of the NMR data in terms of approach-to-equilibrium kinetics (Scheme 2b) gave rate constants for forward (k_1) and reverse (k_{-1}) reactions of *ca.* 3-6 μs^{-1} (half-lives 32–58 h) in the order PF_6^- > NO_3^- > BF_4^- > Cl^- (Table 1 and Figs. S5–S8 in Supporting information).

Table 1
Rate constants (k) and the free energy of activation ($\Delta G^{\ddagger}$) for the conformational interconversion at 288 K.

Complex	k (μs^{-1} [a])		K_{eq}	$\Delta G_{eq}^{\ddagger}$ (kJ/mol [a])		$\Delta\Delta G_{eq}$ (kJ/mol)
	k_1	k_{-1}		$(\Delta G_1)_{eq}^{\ddagger}$	$(\Delta G_{-1})_{eq}^{\ddagger}$	
1·2Cl	3.3 ± 0.1	3.0	1.1	100.67	100.89	0.2
1·2NO$_3$	4.1 ± 0.1	3.8	1.1	100.15	100.33	0.2
1·2PF$_6$	6.0 ± 0.1	5.6	1.1	99.24	99.41	0.2
1·2BF$_4$	3.9 ± 0.2	3.6	1.1	100.27	100.46	0.2

[a] Rate constants (k) and free energies (ΔG) calculated from ^{1}H NMR spectra in CD_3CN at 288 K (Figs. S5–S8) with Eqs. 1–3 (Supporting information, Section 3.7-Kinetic studies of the interconversion in Supporting information). Forward reaction is conversion of *boat*/*twist-boat* to *chair* form.

As shown in Figs. S14 and S15 (Supporting information), two sets of signals were observed in the 2D [^{1}H, ^{1}H] NOESY NMR spectra of **1·2Cl** or **1·2CF$_3$SO$_3$** one week after dissolution in DMSO–d_6 solution, indicating the co-existence of both of *chair*- or *boat*-configurational isomers in each solution. Near-complete assignments of NOESY NMR spectra of **1·2Cl** and **1·2CF$_3$SO$_3$** were achieved, details are listed in Tables S9 and S10 (Supporting information). Characteristic NOE cross-peaks allowed identification of the *boat* or *chair* isomers in solution (Table S11, Fig. S16 in Supporting information). For example, the intensities of NOE cross-peaks for Hi-Hf, Hf-Hl, He-Ha and He-Hb, or Hf-Hl, Hd-Hi, Hi-Hf, He-Ha, He-Hb and Hf-Hj differ for *boat* and *chair* isomers of **1·2Cl** or **1·2CF$_3$SO$_3$**.

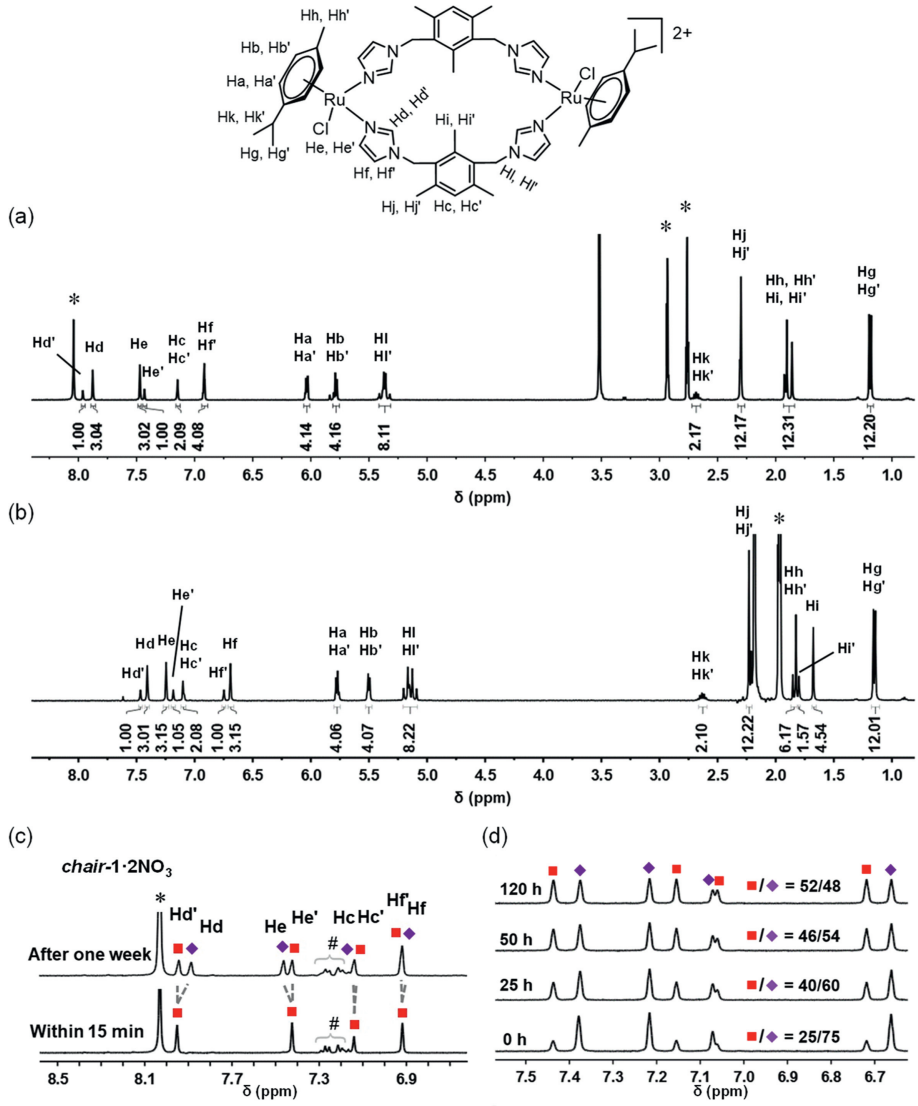


Fig. 3. 400 MHz ^{1}H NMR spectra of (a) as synthesized **1·2NO$_3$** freshly dissolved in DMF-d_7, and (b) fresh in CD_3CN. Low field region for (c) crystals of ***chair*-1·2NO$_3$** soon after dissolution in DMF-d_7, and after 1 week at ambient temperature, and (d) time dependence for as-synthesized **1·2NO$_3$** over 120 h at 288 K in CD_3CN. (a, b) The sensitivity of the chemical shifts of backbone peaks for Hc-Hf (*boat* ◆) and Hc'-Hf' (*chair* ■) is evident. (c) Slow conversion of *chair* to 1:1 equilibrium mixture of *chair* and *boat* forms, and (d) the reverse conversion of *boat* to *chair*. * = DMF-d_7/CD_3CN; # = toluene.

Next we carried out NMR titration experiments to determine whether there are specific interactions between anions and the macrocyclic ring as observed in the X-ray crystal structures (Figs. S17–S23 in Supporting information). As seen in Figs. S17–S19 (Supporting information) gradual low field shifts for the imidazole Hd and Hd' protons of both *boat* and *chair* forms arose from addition of LiCl to **1·2NO$_3$**, **1·2PF$_6$** or **1·2CF$_3$SO$_3$** in DMF-d_7, amounting to *ca.* 0.6 ppm with 5 equiv. of LiCl, giving shifts close to those for **1·2Cl**, but very small shifts for other peaks. The titration did not reach the saturation point before using 40-fold excess of chloride anions (Figs. S24A-Cb in Supporting information). The most notable change was the chemical shift of the characterized imidazole C–H proton involved in the formation of C–H···Cl^- hydrogen-bonds. A Job's plot analysis showed a maximum change in chemical shift at a mole fraction of 0.333, thus indicating a 1:2 binding stoichiometry. (Figs. S24A-Ca in Supporting information). The apparent Cl^- binding constants (L/mol) were determined using WinEQNMR2 software [28] to be $K_{11} = 131.7$ for **1·2NO$_3$**, $K_{11} = 142.8$ for **1·2PF$_6$** and $K_{11} = 508.3$ for **1·2CF$_3$SO$_3$** (Table S12 in Supporting information). Second Cl^- complexation constants K_{12} were much smaller, *ca.* 11 L/mol (Table S12). In the reverse titration of **1·2Cl** with $LiNO_3$, >200 equiv. were necessary to regenerate the higher field shifts of Hd and Hd' for **1·2NO$_3$** (Fig. S20). Similarly addition of *ca.* 70 equiv. of $CF_3SO_3^-$, 40 equiv. of PF_6^- to **1·2Cl** in DMF-d_7 were required to convert the chemical shifts of Hd and Hd' to those of **1·2CF$_3$SO$_3$** and **1·2PF$_6$**, respectively (Figs. S21 and S22). Their binding constants are listed in Table S13 (Supporting information). The best fit to the titration data using a 1:2 binding model (Figs. S24D-F) yielded association constants of $K_{11} = 55.8$, 146.9 and 103.7 for NO_3^-, PF_6^-, and $CF_3SO_3^-$ anions, respectively (Table S13). Similar to the Cl^- titration, the second complexation constant K_{12} was much weaker. The trend for binding constants reflects the strength of anion binding to the macrocycle in the order $Cl^- \sim PF_6^- > CF_3SO_3^- > NO_3^-$, a dependency on their shape, size and H-bonding capability. Anion titrations with LiCl in Figs. S17–S19 under the same conditions as for 1·2Cl, led to gradual low-field shifts for the imidazole Hd and Hd' protons of both *boat* and *chair* forms on addition of LiCl to **1·2NO$_3$**, **1·2PF$_6$** or **1·2CF$_3$SO$_3$** in DMF-d_7, amounting to *ca.* 0.6 ppm with 5 equiv. of LiCl, giving shifts close to those for **1·2Cl**, but with very small shifts for other peaks.

Next we used computational modelling to gain insight into the mechanism of the *boat*/*chair*-configuration interconversions. Ex-

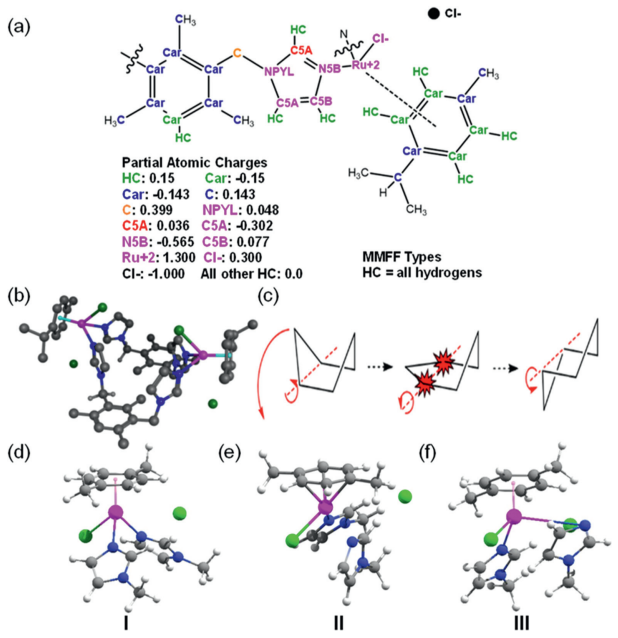


Fig. 4. (a) MMFF atom typing and unique partial charges for **1·2Cl**. (b, c) Interconversion of the *boat-* and *chair-forms* through the rotation. (d-f) Computational transition states for the conformational interconversion. **I**: [Ru(η^6–1,4-dimethylbenzene)(methyl-imidazole)Cl]Cl model; **II**: Ru-N bond dissociation model; **III**: Ru-N bond reforming model.

ploring the configurational space of a moderately large, potentially flexible system like **1·2Cl** or **1·2CF$_3$SO$_3$** using quantum chemistry is challenging. In this case, the LFMM method was employed by extending the force field developed for monometallic Ru-arene complexes [29–31] to include imidazole ligands (Fig. 4 and Fig. S25 in Supporting information). Remarkably, the energy difference among LFMM-optimized ***boat*-1·2Cl** and ***chair*-1·2Cl**, ***boat*-1·2CF$_3$SO$_3$** and ***chair*-1·2CF$_3$SO$_3$** configurations is 0.5 kJ/mol, in excellent agreement with the NMR experiments (Fig. S25, Table 1). As shown in Table S11 and Fig. S16, the NOE cross-peak distances of *boat* or *chair* isomers in **1·2Cl** or **1·2CF$_3$SO$_3$**, are in good agreement with the corresponding distances from the X-ray structures and models. In particular, characteristic NOE cross-peaks allow identification of the ***boat*-1·2Cl** and ***chair*-1·2Cl** isomers in solution, Table S11 and Fig. S16a. However, while broadly similar to the experimental X-ray structures, the LFMM geometries are different and hence the energetic agreement must be treated with caution. Nevertheless, the overall performance of the LFMM force field is sufficiently good to assert that LFMM calculations produce meaningful, although qualitative, results (Figs. S16, S25 and Table S11).

Inspection of the LFMM models revealed that any attempt to convert *boat-form* to *chair-form* structures without rupturing the macrocyclic ring would lead to very high energy intermediates. Essentially, as one end of the *boat-form* structure needs to rotate around a 'hinge' line between the two methylene groups, which connects imidazole and mesityl groups (Figs. 4b amd c), the carbon atoms at the hinge points need to invert. This requires passing through a planar configuration, which is clearly not viable. In this case, the macrocycle must be broken, most likely *via* fission of one of the Ru-N bonds.

Density functional theory (DFT) was used to examine this possibility because, as is common to any valence force field (FF), LFMM cannot handle bond-making/bond-breaking [32]. The Ru-N dissociation energy was computed for a model system [Ru(η^6–1,4-dimethylbenzene)(methyl-imidazole)Cl]Cl (**I**, Fig. 4d). A linear transit calculation using one of the Ru-N distances as the constrained variable resulted in an energy profile, which shows a maximum at ~3 Å followed by a local minimum at ~3.6 Å (Fig. S26 in Supporting information). A full transition state search starting from the maximum of the linear transit converged to a TS (single imaginary mode = −97 cm^{-1}, Fig. S27 in Supporting information) with a Ru-N distance of 2.62 Å at an energy 87 kJ/mol higher than **I** (at the BP86D3/TZVP/COSMO (acetone) level of theory) [33–36]. The subsequent local minimum suggested by the linear transition displays a η^2–type interaction from the C=C double bond of the imidazole to the Ru center, while the linear transit suggests a progressive increase in potential energy as the Ru-N bond is stretched to infinity leading to a dissociation energy of ~180 kJ/mol. There is a significant entropy contribution included (~70 kJ/mol) for the dissociative process, and the computed free energy barrier is ~110 kJ/mol (**II**, Fig. 4e), which compares favorably with the NMR experimental measurements (102.8–104.5 kJ/mol) (Table 1). Once the Ru-N bond breaks, both imidazoles (disconnected and attached), are relatively free to rotate from their *boat* to *chair* forms. The C(phenyl)-C(H$_2$) rotational barrier is estimated at ~38 kJ/mol based on MMFF (Merck molecular force field) calculations using the Molecular Operating Environment implementation (Fig. S28 in Supporting information). The fragment can also freely rotate around the other C(phenyl)-C(H$_2$) bond, which orients the coordinatively unsaturated Ru center correctly for reforming the Ru-N bond and thus reconstituting the metallamacrocyclic ring (**III**, Fig. 4f). These findings are likely to stimulate investigations of dynamic configurational changes which might occur *via* metal-ligand bond breaking and reformation in other second-row metallamacrocycles, or the even more kinetically-labile first-row transition metals.

Crystal structures revealed H-bonding between solvent (H$_2$O/CH$_2$Cl$_2$) and isomers. Hd/Hd' protons in DMF showed downfield shifts *vs.* acetonitrile (polarity-dependent), while DMSO titration caused upfield shifts (weak interactions, no coordination). Computed isomerization barriers (~110 kJ/mol) matched NMR data (103–105 kJ/mol), consistent with macrochelate ring-opening mechanisms. Solvent polarity influenced local electronic environments but did not alter isomer ratios, indicating H-bonding stabilizes conformations without driving interconversion.

This discovery of a new class of metallamacrocycles with stable, but interconvertible, *boat* and *chair* configurations capable of distinctly different dinuclear coordinative binding as well as hydrophobic and H-bonding interactions with the backbone, suggests applications for induced fit recognition of biological targets such as proteins and DNA, and therapeutic activity [24,37–39]. In comparison, literature reports show that other macrocyclic configuration changes can result from either of the metal centers [40–42]. Hydrolysis of both Ru-Cl bonds in **1·2Cl** appears to be facile in aqueous media to give mono- and bis-aqua adducts (Figs. S29–S31 in Supporting information), and mono- and bis-9EtG (9-ethylguanine) adducts have been characterized by ESI-MS (Fig. S32 in Supporting information), which raises the possibility that *boat* and *chair* isomers might have selective GG recognition sites on DNA. This study focuses on the synthesis, characterization, and novel dynamic interconversion behavior of a new class of organo-metallomacrocycles. While preliminary experiments suggest there might be potential biological applications, systematic biological investigations remain to be conducted. In future work, we plan to further explore these through a series of biological experiments, such as cellular activity assays and target-binding validation.

Declaration of competing interest

The authors declare that they have no known competing financial interests or personal relationships that could have appeared to influence the work reported in this paper.

CRediT authorship contribution statement

Yaqiong Kong: Writing – original draft, Project administration, Methodology, Investigation, Formal analysis, Data curation. **Yan Su:** Writing – original draft, Methodology, Investigation, Formal analysis. **Yong Qian:** Visualization, Resources, Methodology. **Robert J. Deeth:** Methodology, Investigation, Formal analysis. **Isolda Romero-Canelón:** Validation, Software, Formal analysis, Data curation. **Zhi Su:** Validation, Supervision, Methodology, Investigation, Formal analysis. **Hong-Ke Liu:** Writing – review & editing, Supervision, Methodology, Funding acquisition, Conceptualization. **Peter J. Sadler:** Writing – review & editing, Supervision, Resources, Funding acquisition, Conceptualization.

Acknowledgments

This work was funded by the Original Exploration Program and General program of National Natural Science Foundation of China (Nos. 22350001, 21977052, 22077066). PJS thanks Anglo American and EPSRC (No. EP/P030572/1) for funding platinum group metals (PGM) research in his laboratory. Yaqiong Kong thanks the Natural Science Foundation of Anhui Higher Education Institutions (No. 2022AH051716).

Supplementary materials

Supplementary material associated with this article can be found, in the online version, at doi:10.1016/j.cclet.2025.111375.

References

[1] S. Swaminathan, R.J. Deepak, R. Karvembu, Coord. Chem. Rev. 491 (2023) 215230.
[2] T.R. Steel, F. Walsh, A. Wieczorek-Błauż, M. Hanif, C.G. Hartinger, Coord. Chem. Rev. 439 (2021) 213890.
[3] G. Xu, C. Li, C. Chi, et al., Nat. Commun. 13 (2022) 3064.
[4] S.Y. Lee, C.Y. Kim, T.G. Nam, Drug Des. Dev. Ther. 14 (2020) 5375–5392.
[5] Y. Cheng, X. Zhang, G. An, G. Li, Z. Yang, Chin. Chem. Lett. 34 (2023) 107625.
[6] Y. Cheng, Y. He, J. Zheng, et al., Chin. Chem. Lett. 32 (2021) 1437–1441.
[7] Y. Zhao, X. Wang, Z. Li, et al., Chin. Chem. Lett. 33 (2022) 1065–1069.
[8] V. Brabec, J. Kasparkova, Coord. Chem. Rev. 376 (2018) 75–94.
[9] H.K. Liu, J.A. Parkinson, J. Bella, F. Wang, P.J. Sadler, Chem. Sci. 1 (2010) 258–270.
[10] M. Chrzanowska, A. Katafias, R. van Eldik, Inorg. Chem. 59 (2020) 14944–14953.
[11] E.M. Bolitho, N.G. Worby, J.P.C. Coverdale, et al., Organometallics 40 (2021) 3012–3023.
[12] H. Chen, J.A. Parkinson, S. Parsons, et al., J. Am. Chem. Soc. 124 (2002) 3064–3082.
[13] M. Hirahara, H. Nakano, K. Uchida, R. Yamamoto, Y. Umemura, Inorg. Chem. 59 (2020) 11273–11286.
[14] N. Kishida, K. Matsumoto, Y. Tanaka, et al., J. Am. Chem. Soc. 142 (2020) 9599–9603.
[15] C. Weng, H. Yang, B.S. Loh, M.W. Wong, W.H. Ang, J. Am. Chem. Soc. 145 (2023) 6453–6461.
[16] M. Wills, Top. Curr. Chem. 374 (2016) 14.
[17] H.K. Liu, P.J. Sadler, Acc. Chem. Res. 44 (2011) 349–359.
[18] H.K. Liu, F. Wang, J.A. Parkinson, J. Bella, P.J. Sadler, Chem. Eur. J. 12 (2006) 6151–6165.
[19] J. Wang, Y. Zhang, Y. Li, et al., Inorg. Chem. 61 (2022) 8267–8282.
[20] J. Li, H. Luo, X. Zhu, J. Zhao, T. Chen, Chin. Chem. Lett. 33 (2022) 788–792.
[21] H.Y. Lin, Y.T. Wang, X. Shi, H.B. Yang, L. Xu, Chem. Soc. Rev. 52 (2023) 1129–1154.
[22] P.P. Hua, H.J. Feng, S.N. Lan, F. Aznarez, L.F. Zhang, Chin. Chem. Lett. 36 (2025) 110684.
[23] S.P. Zheng, Y.W. Xu, P.Y. Su, et al., Chin. Chem. Lett. 35 (2024) 108477.
[24] Y. Qin, Q.H. Ling, Y.T. Wang, et al., Angew. Chem. Int. Ed. 62 (2023) e202308210.
[25] Y. Zhao, L. Zhang, X. Li, et al., Proc. Natl. Acad. Sci. U. S. A. 116 (2019) 4090–4098.
[26] S.J. Bao, H.N. Zhang, G.X. Jin, CCS Chem. 6 (2024) 2000–2010.
[27] C. Ma, J. Wang, L. Zhao, et al., CrystEngComm 15 (2013) 10311–10315.
[28] M.J. Hynes, J. Chem. Soc. Dalton Trans. (1993) 311–312.
[29] R. Brodbeck, R.J. Deeth, Dalton Trans. 40 (2011) 11147–11155.
[30] N.P.E. Barry, R.J. Deeth, G.J. Clarkson, I. Prokes, P.J. Sadler, Dalton Trans. 42 (2013) 2580–2587.
[31] Z. Liu, R.J. Deeth, J.S. Butler, et al., Angew. Chem. Int. Ed. 52 (2013) 4194–4197.
[32] P. Comba, T.W. Hambley, B. Martin, Molecular Modeling of Inorganic Compounds, 3rd ed., Wiley-VCH Verlag GmbH & Co. KGaA, Weinheim, 2009.
[33] F. Weigend, R. Ahlrichs, Phys. Chem. Chem. Phys. 7 (2005) 3297–3305.
[34] A.D. Becke, Phys. Rev. A 38 (1988) 3098–3100.
[35] S. Grimme, J. Antony, S. Ehrlich, H. Krieg, J. Chem. Phys. 132 (2010) 154104.
[36] J.P. Perdew, Phys. Rev. B 33 (1986) 8822–8824.
[37] Y. Xu, Y. Dou, Q. Li, et al., Coord. Chem. Rev. 493 (2023) 215320.
[38] H. Sepehrpour, W. Fu, Y. Sun, P.J. Stang, J. Am. Chem. Soc. 141 (2019) 14005–14020.
[39] S. Jin, N. Muhammad, Y. Sun, et al., Angew. Chem. Int. Ed. 59 (2020) 23313–23321.
[40] H. Fu, S. Pramanik, I. Aprahamian, J. Am. Chem. Soc. 145 (2023) 19554–19560.
[41] Z.W. Li, X. Wang, L.Q. Wei, I. Ivanović-Burmazović, G.F. Liu, J. Am. Chem. Soc. 142 (2020) 7283–7288.
[42] C. Wang, L. Xu, Y. Rao, et al., Chem. Asian J. 19 (2024) e202300923.